Journal of Inclusion Phenomena **4**, 1–29. © 1986 *by D. Reidel Publishing Company.*

Shape-Selective Catalysis and Process Technology via Molecular Inclusion in Zeolites

IAN E. MAXWELL
Koninklijke/Shell-Laboratorium, Amsterdam (Shell Research B.V.), P.O. Box 3003, 1003 AA Amsterdam, The Netherlands

(Received: 6 May 1985)

Abstract. The use of zeolites in shape-selective catalysis is a field which has experienced rapid growth in recent years both as regards the development of new concepts and the applications in petrochemical process technology. This review article is intended to introduce the catalytic concepts and process technology involved, with ample use of examples, rather than to provide a comprehensive coverage of the field.

An introduction to the subject matter is given by discussing zeolite composition and structure, active sites for catalysis and diffusion phenomena. The various types of shape selective catalysis are discussed, i.e., reactant, restricted transition state and product selectivity. The process technology discussion covers topics such as catalytic dewaxing, methanol conversion and aromatics synthesis. Finally, future trends are discussed which indicate that there is scope for further exciting developments in shape-selective catalytic chemistry and applications in process technology.

Key words: Shape selective zeolite catalysis, new catalytic concepts, applications process technology, diffusion phenomena.

1. Introduction

1.1. SCOPE

Shape-selective catalysis using zeolites is a field of rapidly growing importance with respect to both the generation of new concepts in catalysis and the application of innovative petrochemical processing technology.

The reactions involved occur within the intracrystalline space of the zeolite catalysts where the pores have dimensions similar to the kinetic diameters of molecules such as simple aromatics and branched paraffins. The often subtle interplay between the zeolite pore structure and the dimensions of reactant, intermediate and/or product molecules provides the basis for shape-selective or molecular-inclusion-directed catalysis.

The scope of this review article will be more directed towards introducing the concepts involved, with ample use of examples, rather than attempting to comprehensively review the entire field. In addition a number of applications of this type of catalysis in petrochemical process technology will be discussed.

1.2. ZEOLITE COMPOSITION AND STRUCTURE

A very brief discussion of the structure and chemistry of zeolites relevant to this review is given. For a more comprehensive discussion of this subject the reader is referred to an excellent book by Breck [1].

Zeolites are crystalline aluminosilicates (synthetic and natural), with a chemical composition which corresponds to the general formula:

$$M^{n+}_{x/n}[(AlO_2^-)_x(SiO_2)_y]_z H_2O$$

where M^{n+} is the cation which balances the negative charge associated with the framework aluminium ions. The framework ions, Si^{4+} and Al^{3+}, are each tetrahedrally coordinated to four oxygen anions. The periodic three-dimensional network, which is so characteristic of zeolites, is formed by linking the (SiO_4) and $(AlO_4)^-$ tetrahedra through shared oxygen ions. These tetrahedra tend to form rings, containing from four to twelve tetrahedral units. Such rings normally form the entrances to channels or cages in zeolites and thus define the pore diameter for a particular structure. The composition pore volumes and pore diameters for a number of common zeolites relevant to this reveiw are given in Table I.

Table I. Composition and pore parameters of some zeolites

Type	Unit-cell composition	Void volume (ml/ml)	Pore diameter (Å)[a]	Thermal decomposition temp. (°C)	Si/Al ratio
Zeolite A	$Na_{12}(AlO_2)_{12}(SiO_2)_{12}$	0.47	4.2	700	1.0
Zeolite X	$Na_{86}(AlO_2)_{86}(SiO_2)_{106}$	0.50	7.4	772	1.23
Zeolite Y	$Na_{56}(AlO_2)_{56}(SiO_2)_{136}$	0.48	7.4	793	2.43
Mordenite	$Na_8(AlO_2)_8(SiO_2)_{40}$	0.28	6.7 × 7.0	1000	5.0

[a] 1 Å = 10^{-1} nm. (Reproduced from [46]).

Zeolites A, X and Y all consist of tetrahedra linked to form cubo-octahedra or so-called sodalite cage units. When these units are linked through four-membered rings, zeolite A is formed (see Figure 1), whereas linking via the six-membered rings results in zeolites X and Y (see Figure 2). The latter two zeolites only differ in the Si/Al ratio.

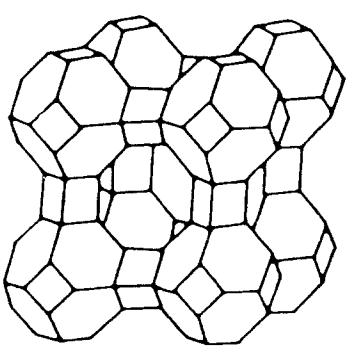

Fig. 1. Schematic diagram of zeolite A (Reproduced from [47]).

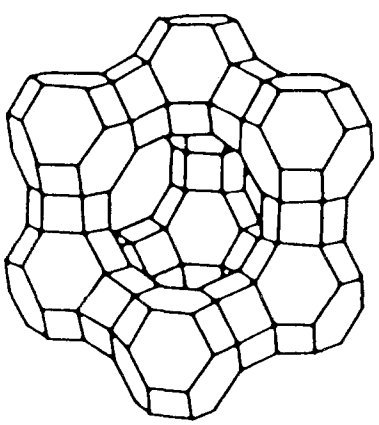

Fig. 2. Schematic diagram of zeolites X and Y (Reproduced from [47]).

Mordenite has a channel-like pore structure in which the basic building blocks consist of five-membered rings. A view of the mordenite structure perpendicular to the main channels is shown in Figure 3.

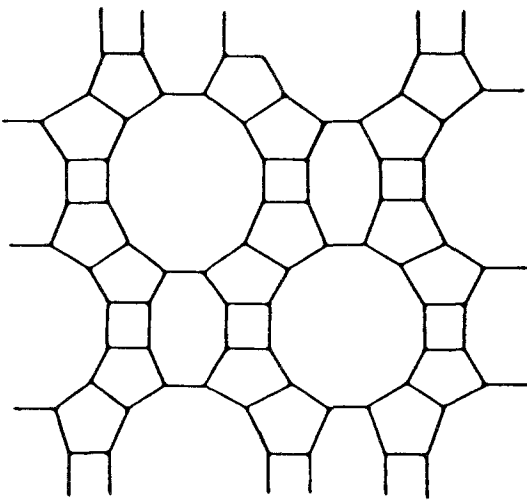

Fig. 3. Section through mordenite structure perpendicular to the main channels (Reproduced from [47]).

In general, zeolites have good thermal stability, but this is further improved by increasing the Si/Al ratio as shown in Table I. The hydrothermal (steam) stability of zeolites also increases with decreasing aluminum content.

Zeolites which are of more interest with respect to shape-selective catalysis include the Chabazite group [2], an example of which is erionite (see Figure 4). Further, the so-called

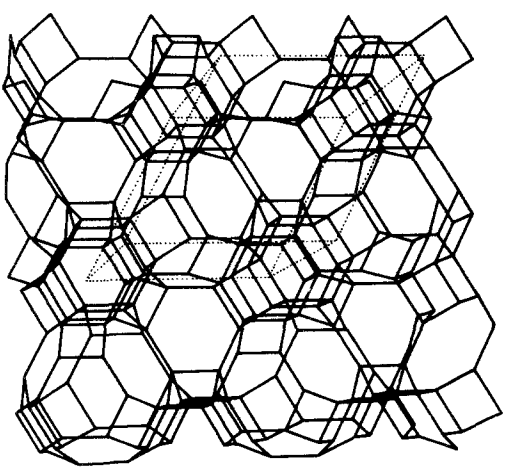

Fig. 4. Schematic diagram of erionite structure viewed along the *c*-axis (Reproduced from *The Atlas of Zeolite Structure Types*, W. M. Meier and D. H. Olson, Verlag AG, Zurich, 1978).

pentasil zeolites are of particular interest and the structures of the end members of this series, ZSM-5 and ZSM-11, are shown in Figures 5 and 6. The pore dimensions of these zeolites are in the range 5.1–5.6 Å which are similar to the critical diameters of simple isoparaffin and substituted aromatic structures. As previously mentioned, this means that diffusivities in the pentasil intracrystalline pores will be highly sensitive to molecular configuration.

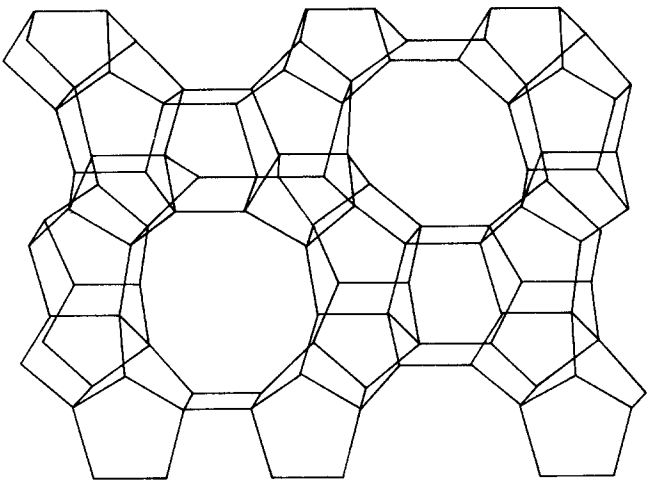

Fig. 5. Schematic diagram of ZSM-5 structure viewed along the *b*-axis (Reproduced from J. Dwyer and A. Dyer, *Chemistry and Industry*, April 1984, p. 237).

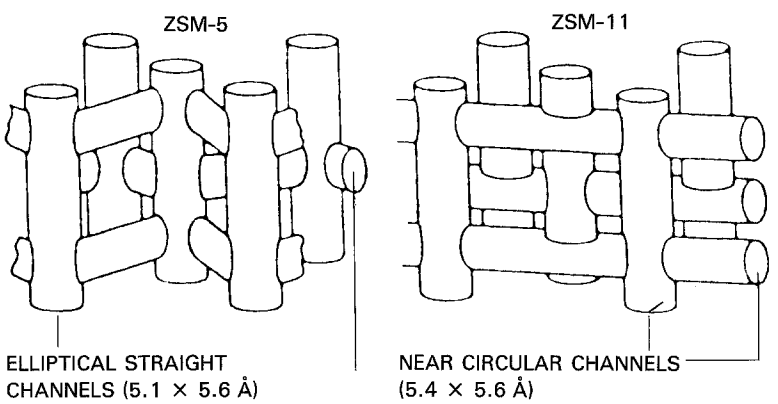

Fig. 6. Channel networks of ZSM-5 and ZSM-11 zeolites (Reproduced from J. Dwyer and A. Dyer, *Chemistry and Industry*, April 1984, p. 237).

In recent years the application of techniques such as selected area high resolution electron microscopy (HREM) has demonstrated that many zeolite structures are in fact imperfect in a crystallographic sense. These imperfections may be localized structural defects, stacking faults or even intergrowths (ordered or disordered) of different zeolite types. For example, Thomas [3,4,5] has provided HREM evidence that the ZSM–5 and ZSM–11 zeolites are most likely the end members of an infinite series of *ordered* intergrowth structures (see

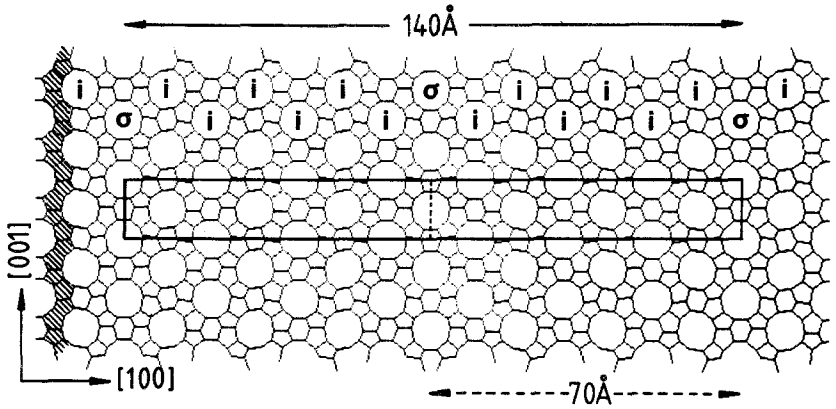

Fig. 7. Schematic skeletal drawing of a ZSM-5/ZSM-11 intergrowth of periodicity along [100] of 140 Å (projected along [010]). Positions of Si (or Al) atoms coincide with line intersections. Adjacent [100] planes related by centres-of-inversion symmetry are indicated by *i* and those related by mirror planes by σ. The shaded chain at the extreme left represents the termination of a single [100] sheet or plane (Reproduced from [5]).

Figure 7). It is highly probable that these types of imperfections have important consequences on the sorptive, diffusion and catalytic properties of zeolites.

1.3. ACTIVE SITES FOR CATALYSIS

The framework charge-compensating cations in a zeolite, which for synthetic zeolites are normally sodium ions, can be exchanged for other cations of different type and/or valency. For most catalytic reactions, particularly those of commercial importance, the zeolites are applied in the so-called acidic form. This acidic function can be introduced into a zeolite in a number of ways, but the most common method is via ion exchange with NH_4^+, followed by thermal decomposition, i.e. $NH_4^+Z^- \rightarrow H^+Z^- + NH_3(g)$.

The so-formed proton or Brønsted acid sites provide a catalytic function which can be used for carbenium ion type catalysis (e.g. catalytic cracking). Acid catalysts based on zeolites have been found to exhibit exceptionally high levels of activity compared to, for example, amorphous silica alumina compositions, and have therefore largely replaced the latter types of catalyst for various applications in the petrochemical industry.

The intriguing question as to the origin of this 'super-activity' exhibited by the zeolite-based catalyst remains. Recent studies by Haag *et al.* [6] have provided more insight into the nature of the acidic sites in zeolites. These workers demonstrated that, for example (Figure 8), with HZSM-5 there was a good correlation between the *n*-hexane cracking activity (α) and the zeolite Al content, even down to values as low as 20 ppm Al. It is noteworthy, as shown in Figure 8, that even at Al levels of about 100 ppm the cracking activity level is comparable with that required for a viable commercial process. The active sites in the zeolite are known to correspond with Al atoms in tetrahedral framework positions, i.e.

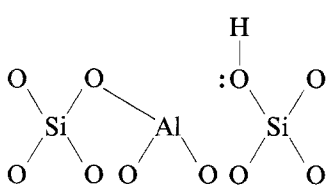

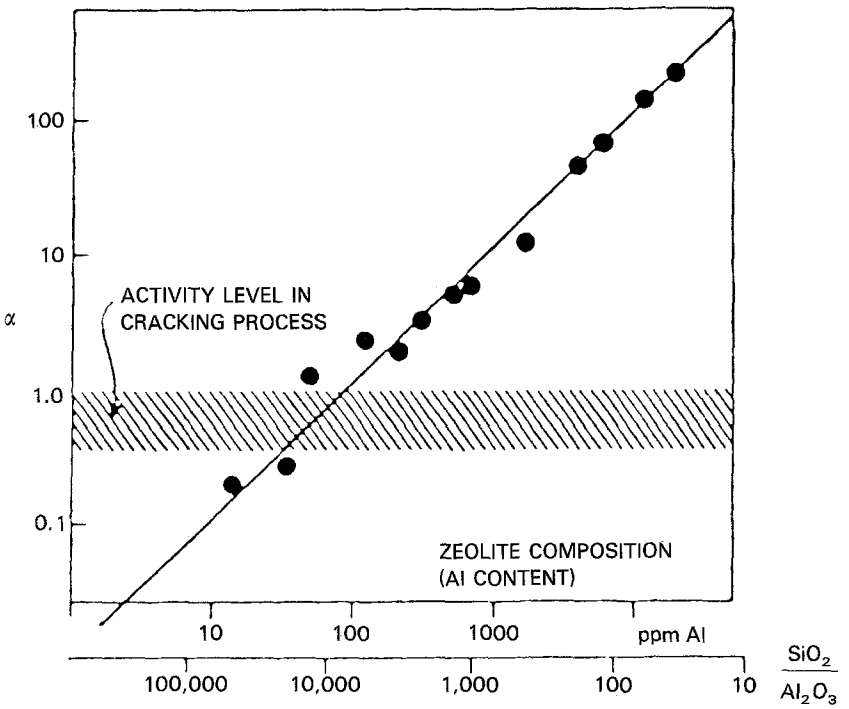

Fig. 8. The hexane cracking activity, α, plotted against the aluminium content of HZSM-5 (Reproduced from [6]).

Until recently, it has been difficult to distinguish between framework and extraneous or non-framework Al. The advent of magic-angle-spinning nuclear magnetic resonance has, however, enabled a distinction to be made between Al in different coordination geometries in zeolites. An example is given in Figure 9, where framework (tetrahedral) and non-framework (octahedral) Al were clearly distinguishable in a sample of zeolite Y [7]. This same

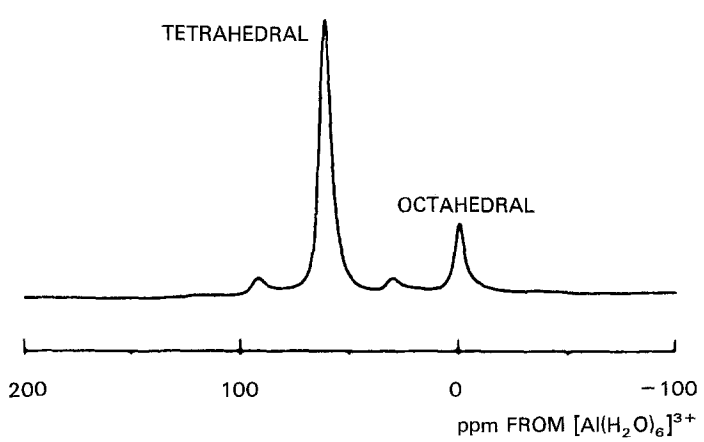

Fig. 9. ^{27}Al Magic angle spinning NMR spectrum of zeolite Y (Adapted from [7]).

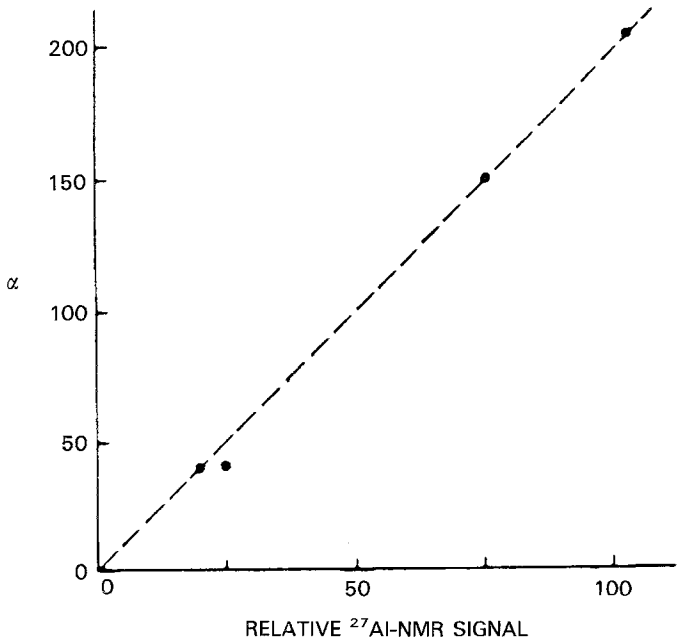

Fig. 10. The hexane cracking activity, α, plotted against the tetrahedral Al NMR signal for HZSM-5 (Reproduced from [6]).

technique was applied to HZSM-5 and a direct proportionality could be shown (see Figure 10) between the *n*-hexane cracking rate (α) and the concentration of framework Al.

Based on the assumption that each tetrahedral Al is associated with one acid site, absolute molecular turnover rates could be determined. Further, turnover numbers (rate per occupied active site) could also be calculated assuming $< 1\%$ steady state occupancy of all Al sites (based on measured first-order reaction kinetics).

The resultant turnover values for C_6 cracking and double-bond isomerization are shown in Table II. It is noteworthy that these values represent remarkably high levels of intrinsic catalytic activity, equivalent to the levels normally encountered in enzyme catalysis.

Table II. The magnitudes of the turnover values for ZSM-5 at 454°C, 100 torr

	Turnover rate (molecules min^{-1} per Al site)	Turnover No. (molecules min^{-1} per active Al site)
n-hexane cracking	0.37	>37
1-hexene cracking	290	>29000
1-hexene double-bond isom.	370000	$\geqslant 4 \times 10^7$

(Reproduced from [6]).

1.4. INTRA-CRYSTALLINE DIFFUSION PHENOMENA

A discussion of intracrystalline diffusion phenomena is essential, since it is precisely the molecular-like dimensions of the zeolitic pore structure which results in shape-selective catalytic properties. The related subject of zeolite inclusion complexes has been recently reviewed by Barrer [8].

1.4.1. *Diffusivity Rates*

Weisz [9] has lucidly placed zeolitic diffusion phenomena in perspective by means of a diffusivity/pore-size diagram (see Figure 11). Zeolites with pore diameters in the range of 4–9 Å are shown to exhibit a region of diffusivity beyond the regular and Knudsen regions, which Weisz has termed the configurational regime. This region, which spans about 10 orders of magnitude in diffusivity, is the regime where molecules must diffuse through spaces of near-molecular dimensions.

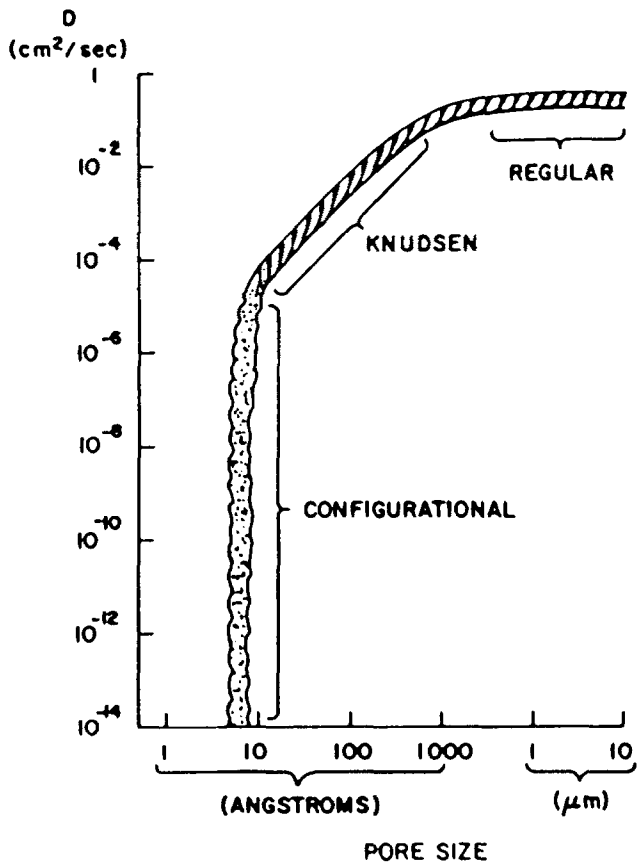

Fig. 11. Molecular diffusivity, D, plotted against pore size aperture (Reproduced from [47]).

In this configurational regime, subtle differences in molecular structure can have a large effect on diffusivity. For example, Riekert [10] has demonstrated for simple paraffins/olefins, that not only chain length, but also decreased carbon-carbon bond mobility, has a marked

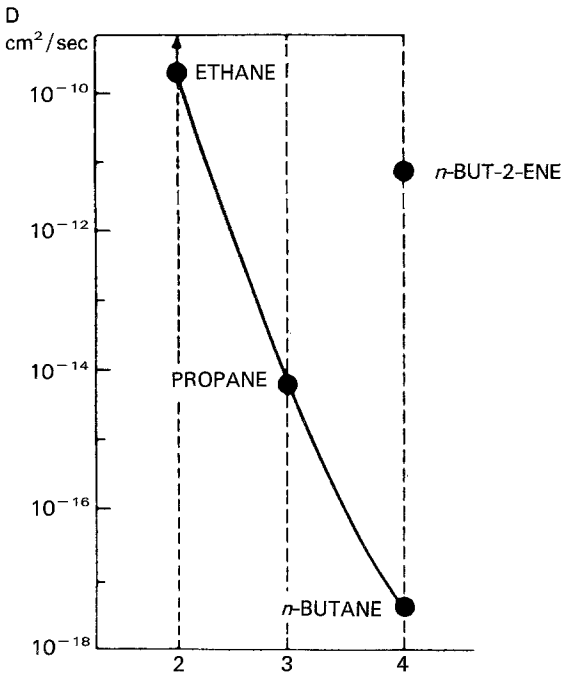

Fig. 12. Diffusivity in zeolite HT as a function of molecular configuration, demonstrating the effect of a single double bond (stiffening) in the 4 carbon-hydrocarbon (Adapted from [26]).

effect on diffusivity. This latter effect results in a reduction of diffusivity by some six orders of magnitude (see Figure 12).

The influence of molecular critical diameter on the effective diffusion coefficient has been nicely demonstrated by counterdiffusion studies using zeolite NaY [11] and is shown in Figure 13. Even more subtle effects are possible, such as a periodic variation in diffusivity with increasing carbon number for *n*-paraffins, as has been observed [12] for zeolite T (see Figure 14).

1.4.2. *Activation Energies for Diffusion*

Although not a great deal of work has been done on the temperature dependence of diffusion in zeolites, at least one likely general trend has been demonstrated. Measurements by Gorring [13] on various alkyl-substituted benzene molecules have shown that for NaZSM-5 (see Table III) the activation energy for diffusion increases as the molecular dimensions approach those of the intracrystalline pore structure. More recently Post [14] has demonstrated from measurements on 2,2-dimethylbutane in ZSM-5 that both the diffusivity and activation energy are independent of the crystallite size.

1.4.3. *Diffusion/Reaction Relationships*

For a reacting species within the intracrystalline pores of a zeolite, the reaction-rate retardation due to diffusion effects can be described by the Thiele modulus concept [14, 15]. For example, the so-called effectiveness factor

$$\eta = \frac{kv}{kv^*} \tag{1}$$

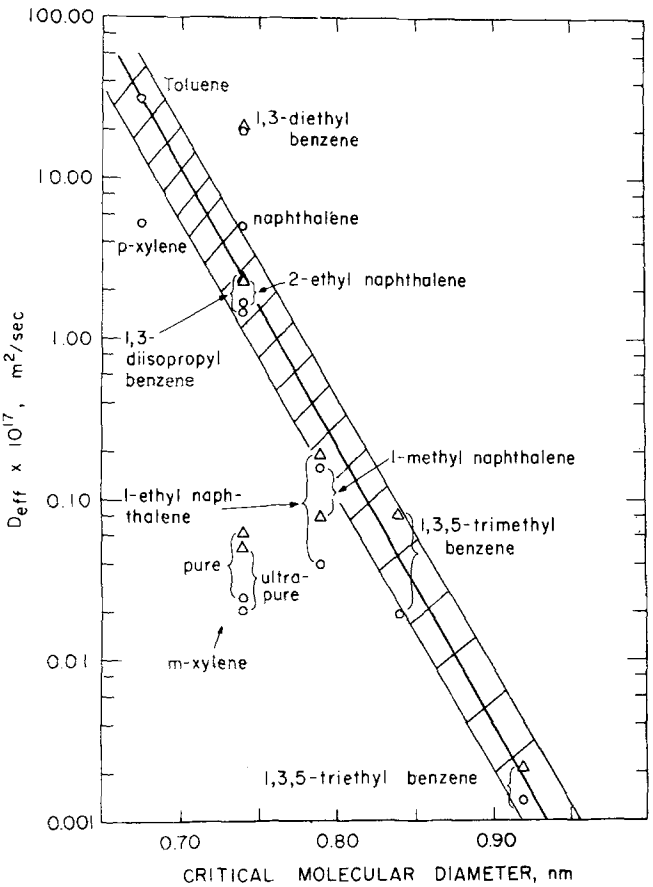

Fig. 13. Diffusivity plotted against critical diameter for various molecules in cyclohexane-saturated NaY (Adapted from [11]).

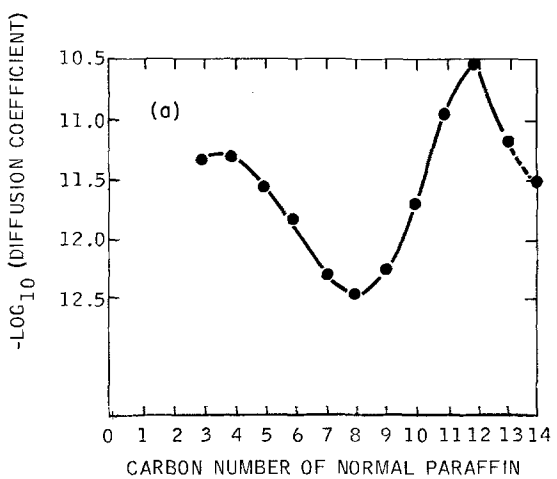

Fig. 14. Diffusivity plotted against carbon number for *n*-paraffins in KT zeolite at 340 °C (Adapted from [11]).

Table III. Activation energies for diffusion in Na-ZSM-5, from sorption studies at 250 °C to 350 °C

	kJ mol^{-1}
o-Xylene	37
m-Xylene	57
t-Butyl benzene	49
1,2,4-trimethylbenzene	57
1,3,5-trimethylbenzene	78

(Reproduced from [46]).

where kv = observed reaction rate constant; kv^* = intrinsic reaction rate constant (i.e. in the absence of diffusion limitations), is related to the Thiele modulus, Φ, for first-order reactions and flat-bed geometry as follows:

$$\Phi = R(k/D)^{1/2} \tag{2}$$

where k = actual observed reaction rate constant divided by the reactant concentration; R = zeolite crystallite radius (i.e. $\frac{1}{2}T$, where T is the thickness of the plate); and D = the reactant diffusivity, whereby

$$\eta = \tanh\Phi/\Phi \tag{3}$$

Thus the effectiveness factor, η, will generally decrease with increasing crystallite size or decreasing reactant diffusivity (see Figure 15). Recent studies by Haag [15] *et al.* and Post

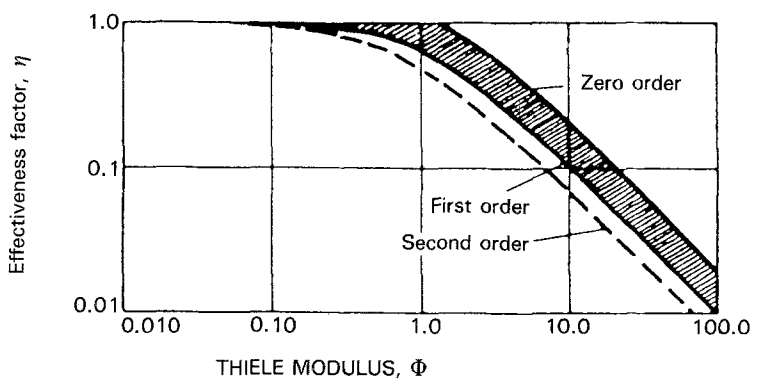

Fig. 15. Effectiveness factor, η, plotted against Thiele modulus, Φ (Adapted from E. G. Derouane, *Intercalation Chemistry*, p. 101, Academic Press, 1982).

et al. [14] have demonstrated that the Thiele concept can indeed be applied to intracrystalline, diffusion-controlled, zeolite-catalysed reactions. For example, based on diffusion measurements and catalytic cracking conversion rates for 2,2-dimethylbutane over zeolite ZSM-5, the Thiele model was shown accurately to describe the relationship between reaction rate and diffusivity (see Figure 16). As will be discussed later, the Thiele concept can also be applied to shape-selective catalysis by introducing a term to describe large diffusivity differences, for example, between different reactant molecules.

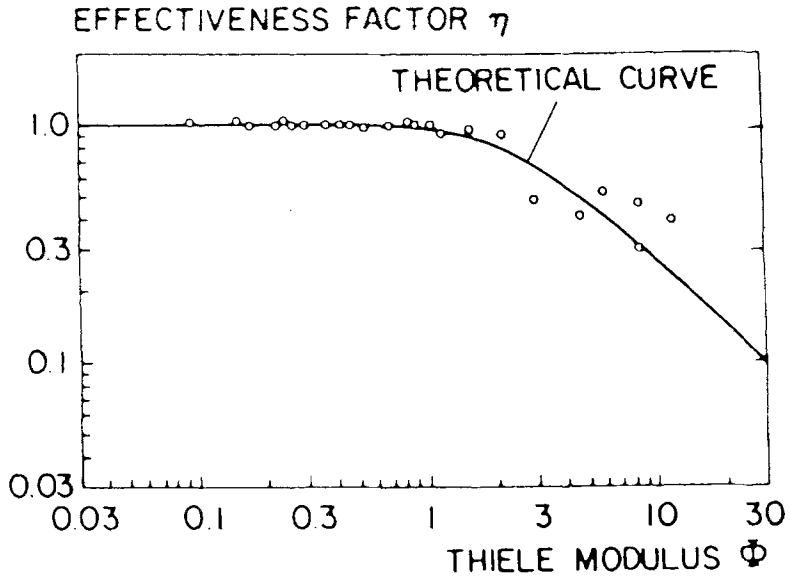

Fig. 16. Application of the Thiele concept for conversion of 2,2-dimethylbutane over HZSM-5 (Adapted from [14]).

2. Shape-Selective Catalysis

As the name suggests, shape-selective catalysis is a phenomenon where the selectivity of a particular reaction scheme can be influenced by the use of catalyst which is capable of 'recognizing' often quite small differences in the shape or configuration of those molecules involved in this process. Zeolitic materials, which exhibit well-defined near-molecular-size pores, good thermal stability and high levels of intrinsic catalytic activity are ideally suited for shape-selective catalysis.

The pioneering studies in this field of catalysis were carried out by Weisz and coworkers [16, 17] in 1960. For example, they demonstrated that the reactivity for dehydration of various isomeric butanols was markedly dependent on the relationship between the reactant shape and the zeolitic pore diameter. As shown in Table IV, only the linear *n*-butanol is capable of

Table IV. Reactant selectivity; dehydration of alcohols

Reactant alcohol	Reaction temperature (°C)	Conversion (wt %)	
		Ca–A (5 Å)	Ca–X (8 Å)
C–C–C–C–OH	260	60	64
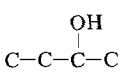	130	0	82
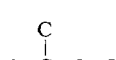	260	<2	85

(Reproduced from [46]).

entering the pores of the CaA zeolite and undergoing a dehydration reaction. This is an example of reactant selectivity where the shape discrimination catalysis is based on the reactant molecules. At least two other types of shape-selective catalysis have since been identified which include restricted transition state and product selectivity. These different types of shape-selectivity will now be discussed in somewhat more detail and illustrated with examples.

2.1. REACTANT SELECTIVITY

Reactant selectivity was the first type of shape-selective zeolite catalysis based on reactant molecular stereochemistry. This is shown schematically in Figure 17, where, for example,

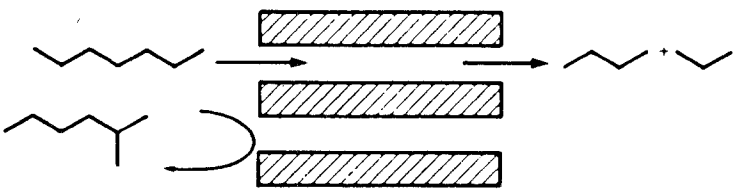

Fig. 17. Schematic diagram demonstrating reactant shape-selectivity (Reproduced from [46]).

normal paraffins are preferentially cracked inside the pores of a zeolite and isoparaffins remain inert simply due to stereochemical pore size limitations. A particularly nice example of reactant selectivity was recently shown for olefin and aromatics hydrogenation using Pt-ZSM-5 [18] (see Table V). A macro-pore non-zeolitic catalyst, Pt-Al_2O_3, was used to provide comparative data. Clearly, the inert behaviour of the more reactive molecules, i.e. 4,4-dimethylhex-1-ene and 2-methylstyrene with the zeolite catalyst is due to reactant shape selectivity. However, the reactivity of these large molecules is intrinsically high, since over the non-zeolitic Pt-Al_2O_3 catalyst the conversion is greater than or equal to their less bulky counterparts, i.e. hexene and styrene.

Table V. Shape selective hydrogenation over Pt-ZSM-5

Catalyst	Temp. (°C)	Pt-Al_2O_3	Pt-ZSM-5
		Hydrogenated (%)	
Hexene	275	27	90
4,4-Dimethylhex-1-ene	275	35	<1
Styrene	400	57	50
2-Methylstyrene	400	58	<2

(Reproduced from [46]).

2.2. RESTRICTED TRANSITION STATE SELECTIVITY

Restricted transition state selectivity is derived from the concept that for a particular reaction pathway this route may be prohibited due to contraints imposed on the molecular dimensions

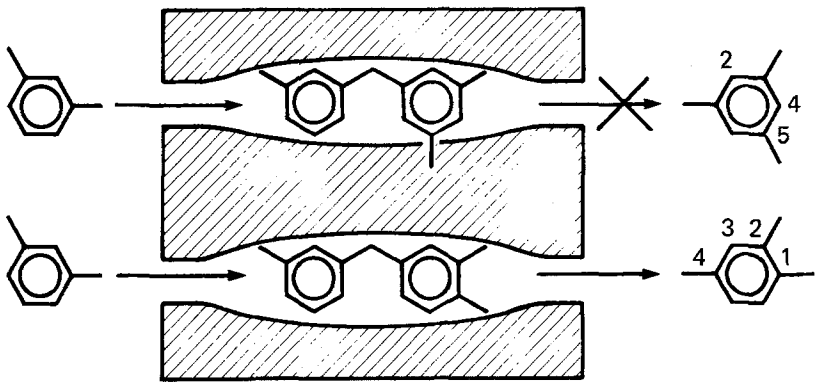

Fig. 18. Schematic diagram demonstrating restricted transition state-shape selectivity (Reproduced from [46]).

of the transition state complex by the the size of the pores of the zeolite. By contrast, typically, both reactants and potential products are able to readily diffuse within the zeolite cavities.

An example of this type of shape-selectivity is given in Figure 18 for the transalkylation of dialkyl benzenes [19]. This reaction involves the transfer of an alkyl group from one aromatic molecule to another through a bimolecular (diphenylmethane) intermediate. As shown in Figure 18, the transition state involving *meta*-dialkyl benzene moieties is substantially bulkier than that containing an *ortho*-dialkyl benzene group. Thus, the formation of the 1,3,5-trialkylbenzene isomer is inhibited, leading to selective formation of the 1,2,4-isomer [20,21].

The interplay that exists between various reaction pathways and the size of the intracrystalline zeolite cavity for the xylene isomerization/disproportionation reactions has been elegantly demonstrated [22]. Under the reaction conditions applied for xylene isomerization, the previously discussed transalkylation or disproportionation reaction may also occur (see Figure 19). Since the disproportionation reaction involves a large bimolecular intermediate, as previously mentioned, and the isomerization occurs via a 1,2-methyl shift, one might expect the ratio of the relative rates of disproportionation and isomerization, k_{DIS}/k_{ISOM}, to be influenced by the size of the zeolite cavities. This is indeed shown to be the case in Figure 20, where the relative rate of disproportionation is found to decrease with decreasing effective

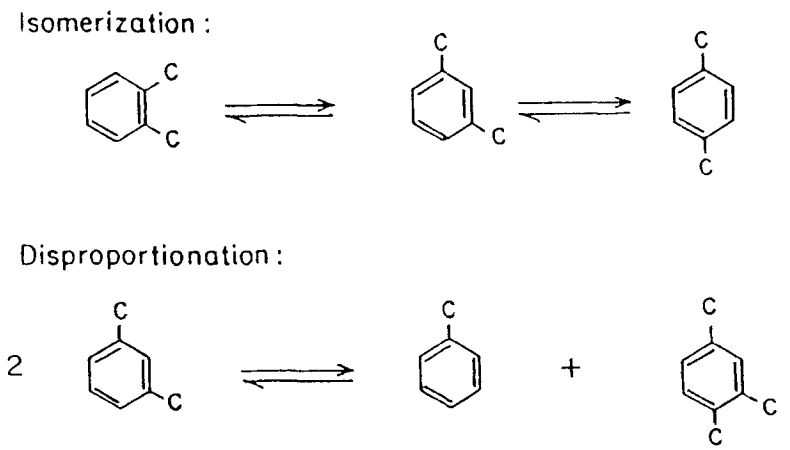

Fig. 19. Xylene isomerization and disproportionation reactions (Reproduced from [22]).

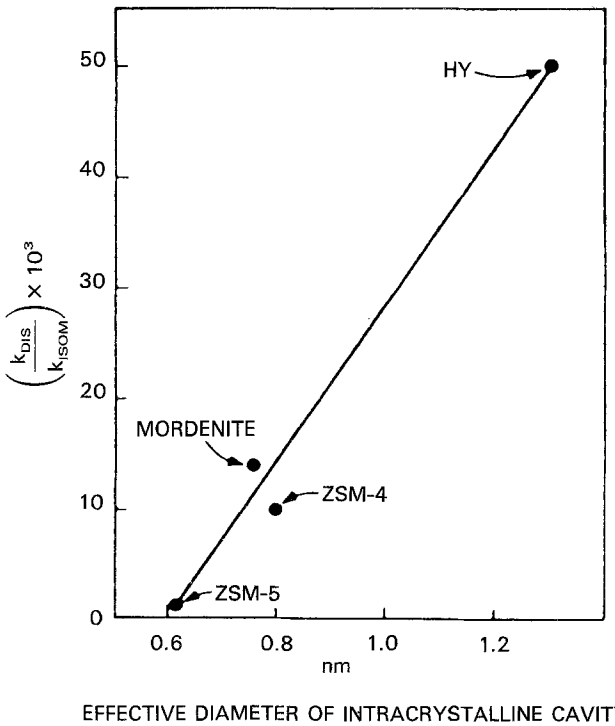

Fig. 20. Selectivity of disproportionation/isomerization reactions against zeolite pore diameter for xylene isomerization (MOR = synthetic Mordenite, reproduced from [22]).

diameter of the zeolite intracrystalline cavity. This is a particularly interesting example of the application of transition-state shape selectivity whereby a potentially undesirable side reaction can be suppressed by the use of a zeolite with the appropriate effective pore diameter.

Another example, which can most likely be described by restricted transition state selectivity, is coke formation in zeolite catalysts. For most acid-catalysed reactions, there is an accompanying deactivation of the zeolite catalyst which occurs to a greater or lesser degree via coke deposition in the intracrystalline pores. The rate of coke deposition depends on the particular reaction, the process conditions and the type of zeolite catalyst.

The rates of coke formation for catalytic cracking of a five-component mixture of paraffins were studied by Rollman [23] *et al.* for a variety of zeolites. As shown in Figure 21, the rate of coking could be correlated with the relative rates of *n*-hexane and 3-methyl pentane cracking, k_{NC_6}/k_{3MP}. This latter parameter, the so-called constraint index, has been shown from previous studies to be a measure of the effective pore diameter of the zeolite [24]. Thus, for a wide range of zeolites it can be shown that for catalytic cracking of simple paraffins the rate of coke formation decreases with reduced effective pore diameter. This may be attributed to transition-state shape selectivity whereby the formation of the bulky, coke-precursor (polyaromatic) molecules is reduced as the intracrystalline pore diameter is decreased.

An understanding of the coke deposition rates in zeolite catalysts is invaluable for evaluating the potential stability performance of such catalysts in commercial operation.

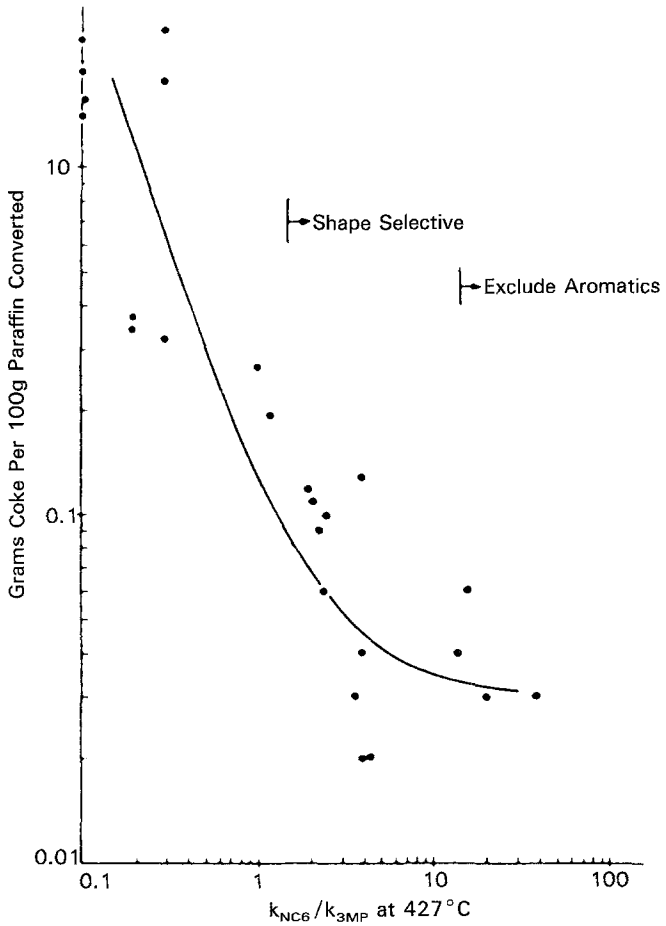

Fig. 21. Coke yield as a function of constraint index (measure of shape-selectivity) for the conversion of paraffins over various acidic zeolite catalysts (Reproduced from [47]).

2.3. PRODUCT SELECTIVITY

Product shape selectivity occurs when a substantial difference in rates of diffusion of product molecules exists within the zeolite intracrystalline space, whereby the product with the highest diffusivity is preferentially recovered. The alkylation of toluene with methanol to selectively form *p*-xylene (Figure 22) is an example where the various alkyl aromatic products have markedly different diffusivities in the zeolite ZSM-5 [22], as shown in Figure 23. The

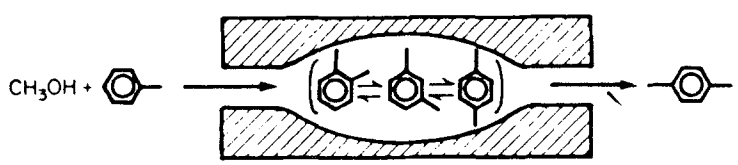

Fig. 22. Schematic diagram demonstrating product shape selectivity (Reproduced from [46]).

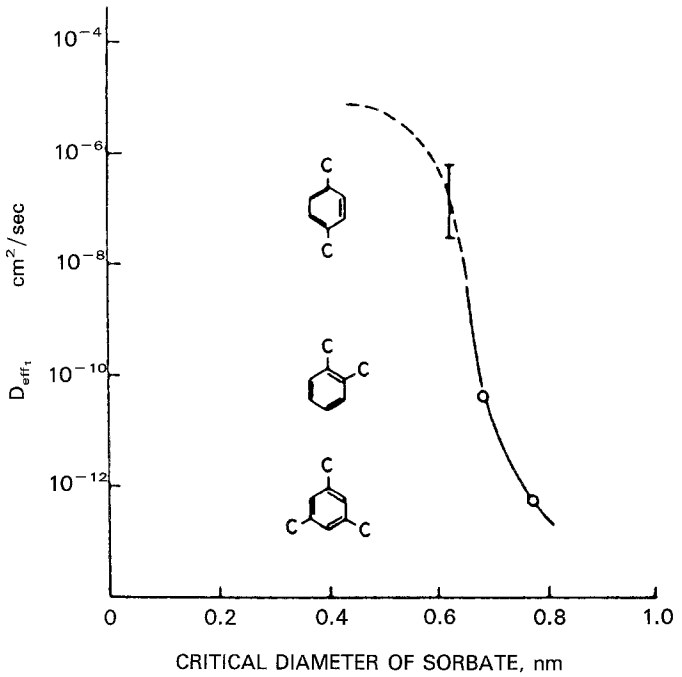

Fig. 23. Diffusivities of some simple aromatic molecules as a function of their critical diameter for ZSM-5 at 315°C (Reproduced from [22]).

diffusivity of *p*-xylene, for example, is a factor of 10^3 greater than than for *m*-xylene, which, provides the basis for the enhanced selectivity towards the *p*-xylene isomer. The observed selectivity is compared to that expected from thermodynamic equilibrium considerations in Table VI.

In fact, as shown in Table VI the *p*-xylene selectivity can be further improved by incorporating phosphorus [25] into the ZSM-5 structure, which apparently reduces the effective pore diameter. The relationship between *p*-xylene selectivity and diffusivity can be described using the previously discussed Thiele concept type of approach [26].

Table VI. Product selectivity using ZSM-5 zeolites

	Catalyst		
	ZSM-5 (3 μ)	ZSM-5 modified with P	Equilibrium
Temperature, (°C)	500	600	
Toluene conversion, (%)	39	21	
Xylenes (wt % of aromatics)	88	90	
Distribution			
p-Xylene	46	97	23
m-Xylene	36	2	51
o-Xylene	18	1	26

(Reproduced from [46]).

Evidently, examples have been chosen where a clear distinction can be made between reactant, restricted transition state and product selectivity; however, for many reactions combinations of the above phenomena will be involved. This is, perhaps, more often the case for industrial applications, where the reactants and products may be quite a complex mixture.

3. Process Technology Based on Shape-Selective Catalysis

The application of shape-selective zeolite catalysis on an industrial scale has been exemplified by rapid growth in recent years. A number of the more important developments will be highlighted.

3.1. CATALYTIC DEWAXING

The first industrial application of shape-selective zeolite catalysis is most likely attributable to the BP Company, who demonstrated the use of the zeolite mordenite for dewaxing lubricating oil base stocks [27]. In essence, the process selectively reduces the molecular weight of normal and slightly branched paraffins (wax components) and thereby improves the cold-temperature properties (e.g. pour point) of the lubricating oil. This process is an example of the application of *reactant* shape-selective zeolite catalysis. The catalyst used is actually bifunctional, containing both hydrogenation and acidic components (i.e. platinum on the hydrogen form of mordenite), whereby the molecular weight reduction of the wax component is achieved via a hydrocracking reaction. The BP process was first applied in a US refinery in the late 1970s [28].

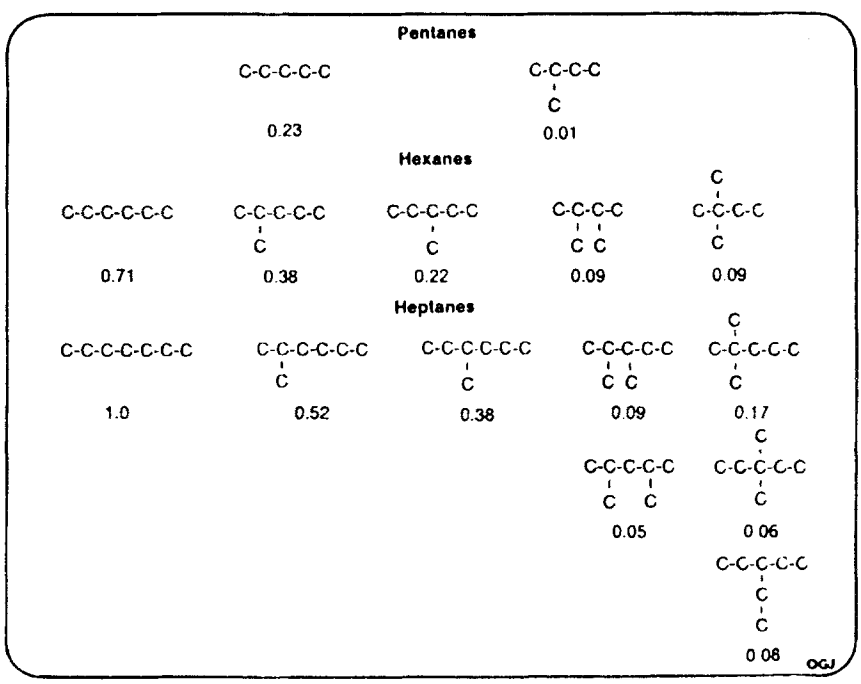

Fig. 24. Relative cracking rates for various paraffins over Mobil catalytic dewaxing catalyst (Reproduced from [29]).

A similar process for dewaxing lube-base stocks has also been developed by Mobil [29] making use of their own proprietary shape-selective catalyst system. The reactant selectivity of the process is demonstrated by the relative cracking rates of various normal and branched paraffins over the Mobil catalyst (see Figure 24).

This type of process can also be extended to improve the cold-flow properties of gas oils [30]. A typical feed and product composition for the Mobil process is shown in Figure 25, where a gas oil pour point reduction of some 85° F (29° C) has been achieved. A rather striking demonstration of the reduction in *n*-paraffin content of the distillate product is shown by means of gas chromatography in Figure 26.

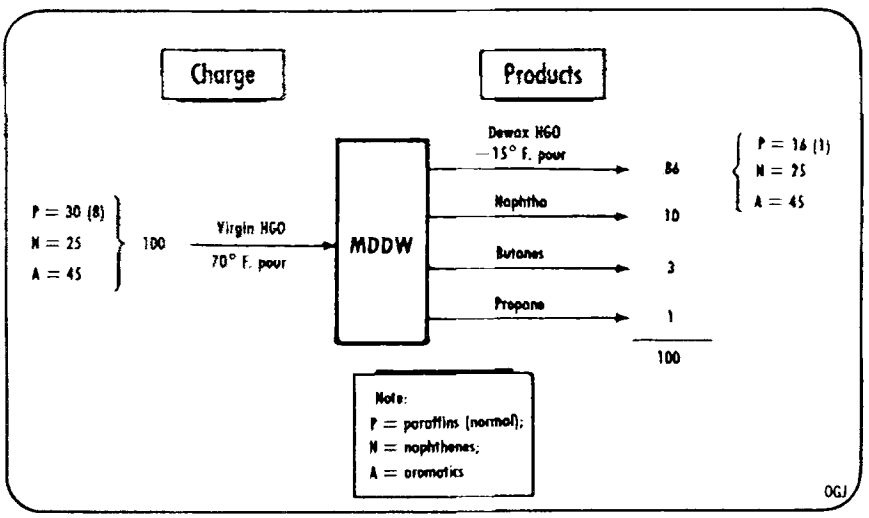

Fig. 25. Change in composition between feed and products for Mobil catalytic dewaxing process (Reproduced from [30]).

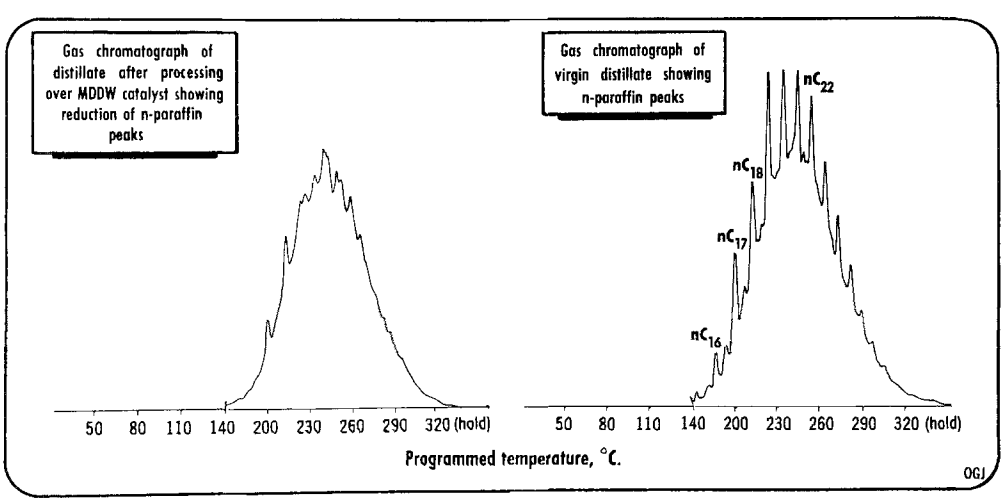

Fig. 26. Demonstration of selective removal of *n*-paraffins following catalytic dewaxing process by means of gas chromatographs of feed and product (Reproduced from [30]).

3.2. SHAPE-SELECTIVE REFORMING

A number of petroleum companies (i.e. Exxon [31], Mobil [32] and Gulf [33]) have studied a shape-selective process for improving octane quality of reformate and gasoline streams. The basic concept is similar to catalytic dewaxing in that *n*-paraffins are selectively hydrocracked to light hydrocarbons, whereby the octane number of the gasoline is upgraded. This process therefore also constitutes an example of *reactant* shape-selective catalysis.

An improvement of this process was recently described, whereby a shape-selective catalyst of medium pore dimensions, such as ZSM-5, was applied [34]. As previously discussed (Figure 24), for the ZSM-5 type catalyst there is a marked variation in cracking rates for various normal and branched paraffins. This phenomenon is most advantageous in selective reforming, since, as shown in Figure 27, the most reactive paraffins have the lowest research octane numbers and vice versa.

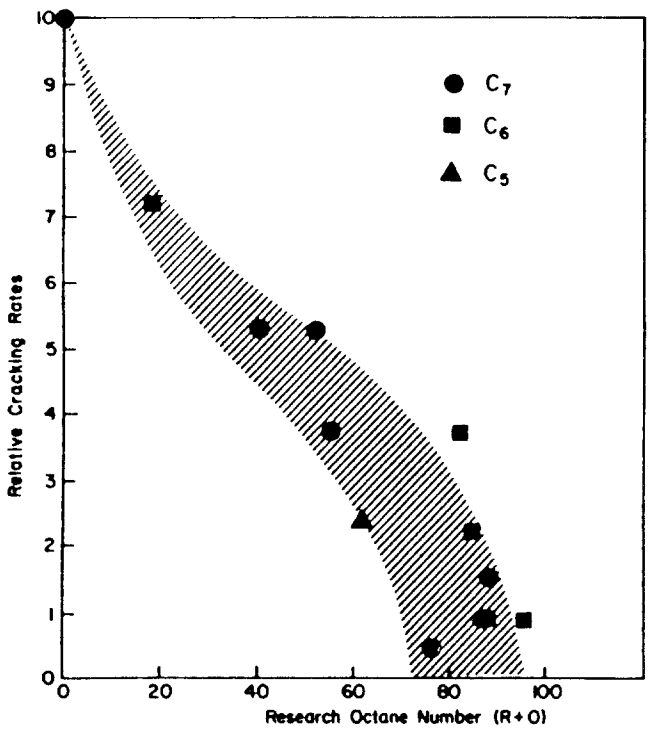

Fig. 27. Relative cracking rates *vs.* research octane number for C_5–C_7 paraffins (Reproduced from [26]).

A further advantage of ZSM-5 compared to, for example, the smaller-pore erionite catalyst is demonstrated in Table VII, where the former zeolite is capable of reacting olefinic fragments of paraffin cracking (in the absence of hydrogen) with aromatics to produce alkylaromatics and therefore increased gasoline yields. These alkylaromatics will, in turn, be limited in degree of substitution and reaction rates by the product diffusion constraints within the ZSM-5 intracrystalline space. For example, the rate of alkylation of benzene was found to be considerably faster than for toluene. By contrast, this situation is reversed for larger-pore zeolites such as faujasite [35].

Table VII. Comparison of paraffin and aromatics alkylation over Erionite and ZSM-5

	Wt. Conversion	
	Erionite	ZSM-5
n-Hexane	92	98
2-Methylpentane	7	56
Benzene	3	16

(Reproduced from [34]).

Another feature of this catalyst system is the relatively low rate of deactivation due to the suppression of coke forming reactions. The above modified reforming process provides an example, whereby all three types of shape-selective catalysis (i.e. reactant, restricted transition state and product selectivity) are operative.

3.3. METHANOL TO GASOLINE AND RELATED PROCESSES

The discovery of the remarkable catalytic capability of the ZSM-5 zeolite to selectively convert methanol into hydrocarbons and water, whereby the hydrocarbons are predominantly in the gasoline boiling range (C_4 to C_{10}), captured the imagination of both the scientific and industrial catalysis communities [35, 36, 37]. The overall stoichiometry of the reaction may be described as follows:

$$x\ CH_3OH \rightarrow (CH_2)_x + x\ H_2O\ .$$

However, the catalytic chemistry involved in converting a one-carbon compound into, primarily, gasoline is quite complex and it is now apparent that the shape-selective properties of the ZSM-5 catalyst play an important role.

The reaction path [35, 36, 38] is shown in Figure 28, where the initial step involves reversible dehydration of methanol to dimethylether followed by further dehydration of both oxygenates to form light olefins. These olefins in turn oligomerize to heavier olefins and then further rearrange to paraffins, cycloparaffins and aromatics.

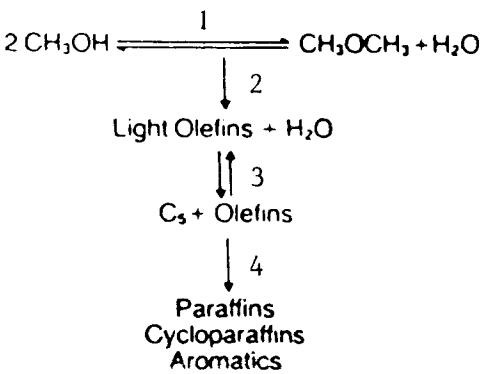

Fig. 28. Reaction pathway for methanol conversion over the HZSM-5 catalyst (adapted from [36]).

The shape-selective behaviour of the catalyst is demonstrated by the fact that almost no hydrocarbons are found higher than C_{10}, thus resulting in a high gasoline selectivity.

Diffusion measurements on ZSM-5 for various C_6 to C_{10} hydrocarbons [35], as shown in Figure 29, demonstrate a dramatic decrease in diffusion coefficients with increasing carbon number and molecular size. Thus, the remarkable cut-off in the carbon number of the product at about C_{10} can be attributed to *product* shape-selective catalysis.

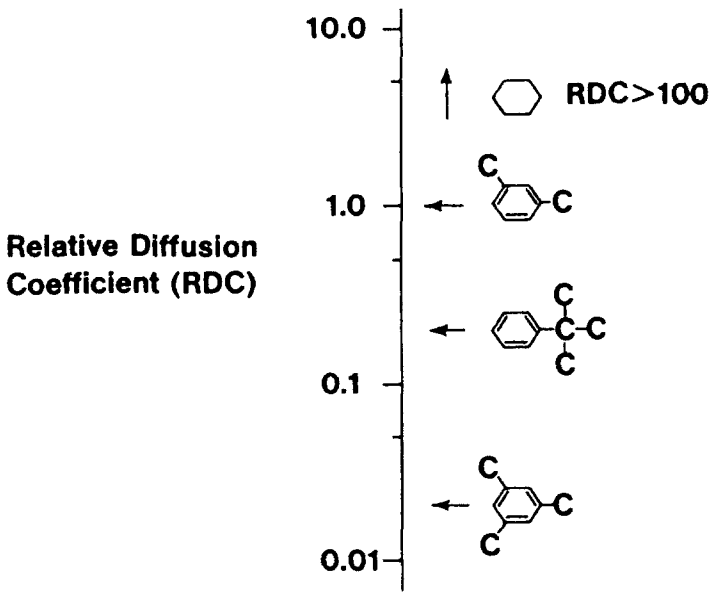

Fig. 29. Relative diffusivities of simple aromatic molecules in ZSM-5 at 350°C (Reproduced from [35]).

The first commercial plant based on the above process technology is currently under construction in New Zealand, where there is an abundance of natural gas but a shortage of crude oil. The basic catalytic chemistry involved, as shown in Figure 28, has been extended to a broader range of feedstocks. These include oxygenates other than methanol [39], synthesis gas ($CO + H_2$) [40] and even biomass compounds (e.g. corn oil, castor oil) [4].

Further, by careful choice of reaction conditions, various consecutive reactions steps can be suppressed, thereby producing primarily intermediate products. For example, a high yield of C_2–C_5 olefins can be obtained from methanol under the appropriate reaction conditions [42,43] (reactions 1 and 2, Figure 28). The light olefins thus formed can be further oligomerized over the same ZSM-5 catalyst to give primarily higher-molecular-weight olefins under different (milder) reaction conditions [44] (reactions 1, 2 and 3, Figure 28). The low aromatic content and minimal branching of the product formed by the above reaction reflects the shape-selective constraints of the ZSM-5 catalysts. It is likely that for this reaction both *transition state* and *product* shape-selective mechanisms are operative, a general scheme [26] is given in Figure 30, indicating the broad scope of this catalysis in terms of both feedstock choice and products.

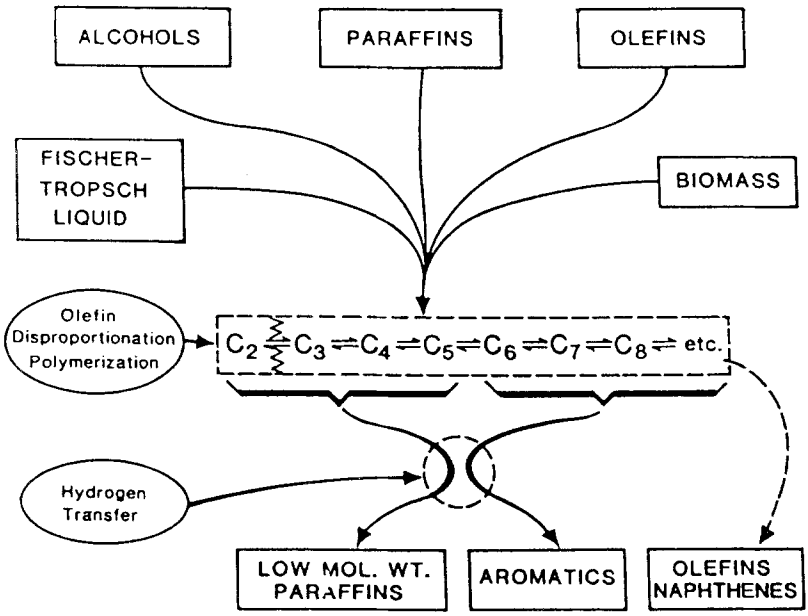

Fig. 30. Mechanistic scheme for conversion of a variety of feedstocks to aromatics over the HZSM-5 catalyst (Reproduced from [22]).

3.4. AROMATICS SYNTHESIS

The synthesis of aromatic hydrocarbons is of considerable importance in the petrochemical industry since these molecules are used as basic building blocks, particularly for the manufacture of synthetic polymers. Often a specific substituted aromatic molecule is required as polymer feedstock, e.g. *p*-xylene, and thus a highly selective synthesis to such a molecule is desirable. In recent years, shape-selective zeolites, in particular ZSM-5 [22], have shown considerable potential in providing a selective means of synthesizing or transforming aromatic hydrocarbons into highly specific products.

As previously shown in Figure 23 for ZSM-5, the diffusion coefficients [22] for a number of simple alkylaromatic molecules vary over a range of 5 orders of magnitude. Further, these diffusion coefficients correlate with the molecular critical diameters. This provides the basis for the shape-selective catalysis employed in the synthesis of aromatics.

A number of examples of aromatic conversions have already been discussed, e.g. *p*-xylene isomerization/disproportionation and *p*-xylene synthesis from toluene. The reaction schemes involved and relative diffusion rates of various reactant and product molecules for the *p*-xylene synthesis are shown diagrammatically [26] in Figure 31.

In addition to product selectivity, the medium-pore zeolites also offer the opportunity of converting a wider range of feedstocks to aromatics than can be achieved by, for example, the conventional catalytic reforming route. The broad range of feedstocks is indicated in Figure 30, which includes alcohols, paraffins, olefins and biomass [22]. A number of typical product breakdowns for the conversion of methanol, ethylene and isoprene over ZSM-5 [42,22,45] are given in Table VIII.

These studies [45] have shown that a general relationship exists whereby the aromatic yield increases with increasing catalyst temperature and decreasing effective H/C ratio, $(H/C)_{eff}$,

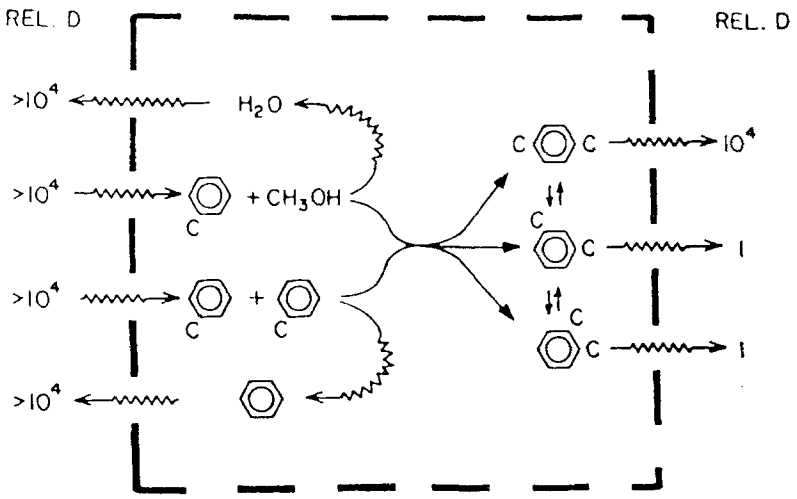

Fig. 31. Mechanistic scheme demonstrating the relative roles of diffusion (reactant and product) and reaction kinetics in *p*-xylene formation either via disproportionation or methanol alkylation of toluene (Reproduced from [22]).

Table VIII. Aromatization of methanol and ethylene with ZSM-5 catalyst at atmospheric pressure

Feed	Methanol	Ethylene		Isoprene
Temperature, °C	371	415	543	482
WHSV	1	4.5	1	1
Effective H/C ratio	2	2	2	1.6
HC products, wt %				
C_1–C_2	2	2	32	10
C_3^+ non-aromatics	62	64	17	22
Aromatics	36	34	51	68
	100	100	100	100
Aromatics, wt %				
A_6	4	2	21	19
A_7	26	18	41	46
A_8	44	36	23	31
A_9	18	37	4	4
A_{10}	8	7	11	–
	100	100	100	100

(Reproduced from [22]).

and $(H/C)_{eff} = (H - 2 * O)/C$, where H, C, and O are the number of these atoms in the empirical formula of the feed. This is reflected in the results shown in Table VIII, where both the temperature and $(H/C)_{eff}$ effects are evident. The composition of the aromatic products in general reflects the *transition state* and *product* shape-selectivity imposed by the zeolite catalyst on the reaction networks.

4. Future Trends

The foregoing sections have provided the reader with a glimpse of the rapid developments that are occurring in this intriguing field of shape-selective zeolite catalysis. Clearly, these developments are not confined to the curiosity of laboratory researchers, but are already having quite some impact in the petrochemical processing industry. In terms of future trends and developments there would appear to be sufficient scope for further exciting shape-selective catalytic chemistry and the applications in process technology are, in general, still in their infancy.

As regards the catalysts, there is enormous scope for engineering subtle variations in both the intracrystalline pore structure and the active catalytic functions. For example, the realization that many zeolites are imperfect [4, 5] and that these structural defects often play an important role in the catalytic properties will likely have considerable implications. It is most likely that techniques will be further developed, not only to measure such defects, but to control their formation in the zeolite structures, thereby designing the desired intracrystalline space. Another approach is to modifying the effective pore dimensions of zeolites by the introduction of various cations via ion exchange. This is demonstrated in Figure 32, where various divalent cations were introduced into the zeolite mordenite in order to steer the selectivity of the xylene *trans*-methylation reaction towards the 1,2,4-trimethylbenzene product [46]. A further example involves the use of P and Mg modified ZSM-5 to improve the *p*-xylene selectivity in the synthesis using toluene and methanol [22] as reactants.

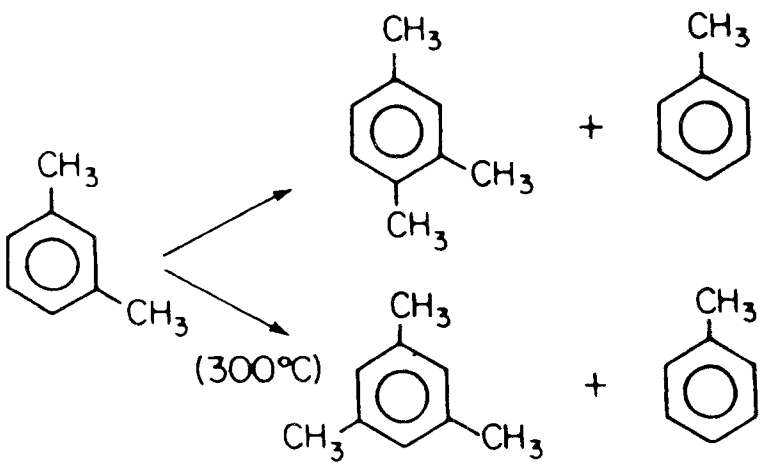

Cation	Ionic radius (Å)	Conversion (%)	Selectivity (%)
H		49	8
Be^{2+}	0.33	29	8
Mg^{2+}	0.62	24	17
Co^{2+}	0.68	23	25
Zn^{2+}	0.74	21	31

Fig. 32. Pore diameter control via exchangeable cations in mordenite for xylene *trans*-methylation reaction (Adapted from [46]).

The application of shape-selective catalysis to a variety of reaction types (e.g. hydrocracking, aromatics formation and transformations, etc.) and a broad spectrum of feedstocks continues to grow. The conversion of biomass constituents such as corn, castor and jojoba oils into high grade gasoline over the ZSM-5 catalyst [41] provides an example of the upgrading of rather exotic feedstocks in a remarkably simple process step making use of shape-selective zeolite catalysis.

Most of the studies to date have been confined to acid-catalysed reactions in which the zeolite catalyst is normally used in the hydrogen form. There would, however, appear to be considerable potential for applying shape-selective zeolites to non-acid-catalysed reactions [47]. In fact, in hindsight, a number of previous studies in this area might perhaps be better interpreted in terms of shape-selective catalysis. An example from our own work is the highly selective cyclodimerization of butadiene to 4-vinylcyclohexene, VCH (Figure 33b) which occurs using Cu^+Y zeolite as a catalyst [48, 49]. By contrast, in homogeneous catalysis a mixture of dimeric and trimeric products is normally obtained (Figure 33a). The remarkable selectivity of the zeolite catalyst might well be attributable to transition-state shape selectivity. It is quite probable that the σ-allyl, π-allyl intermediate (Figure 33c) required to form VCH is significantly less space-demanding than the alternative intermediates such as π,π-allyl complexes necessary for the formation of other oligomeric products.

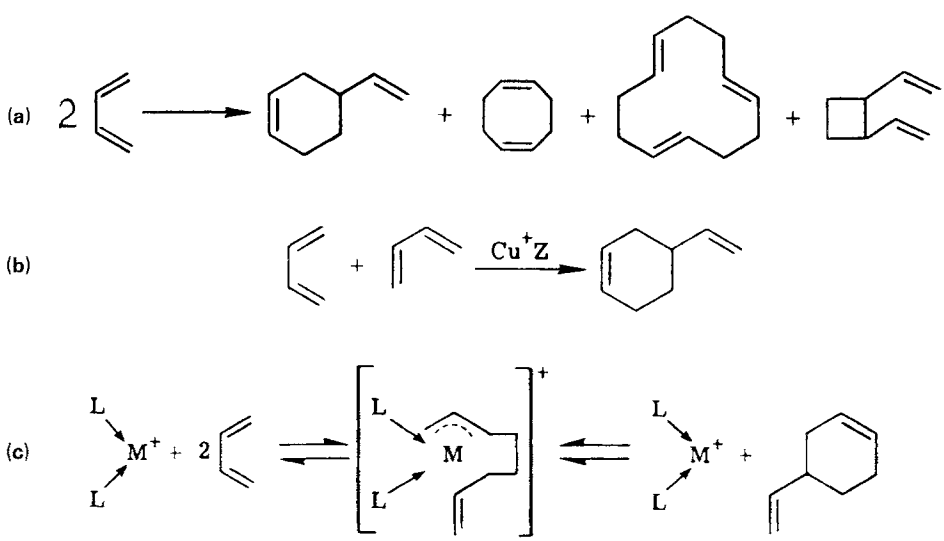

Fig. 33. Butadiene dimerization reactions: (a) possible oligomer products; (b) selective dimerization to vinylcyclohexene (VCH) catalysed by Cu^+-Y zeolite; (c) σ-allyl, π-allyl intermediate, in dimerization to VCH.

Another, more recent example of non-acid catalysis is a study of shape-selective hydrogenation. Dessau [50] has shown that using Pt-ZSM-5, in which the platinum has been carefully dispersed inside the zeolite channels, a variety of linear olefins can be very selectively hydrogenated, whereas the branched olefin isomers also present in the feed (see Table IX) remain virtually unreacted. These few examples of non-acidic shape-selective zeolite catalysis indicate that this is a field of catalytic chemistry which offers quite some scope for future study.

Parallel to the rather exciting experimental studies related to shape-selective catalysis, there is also some initial development occurring with regard to a more theoretical approach. Using

Table IX. Shape-selective competitive hydrogenations

Linear olefin	Branched olefin	Temperature (°C)	% Hydrogenation	
			Linear	Branched
Pent-1-ene	4,4-Dimethylpent-1-ene	300	97	2
Hept-1-ene	4,4-Dimethylpent-1-ene	300	91	1.1
Hex-1-ene	6-Methylhept-1-ene	300	25	2
Styrene	2-Methylstyrene	425	50	2

(Reproduced from [50]).

single crystal X-ray diffraction techniques Seff and co-workers [51] have been able to obtain detailed structural information on inclusion complexes inside the pores of zeolite A. For example, the adsorption complex formed between acetylene(ethyne) and divalent cobalt ions inside the main cavity of zeolite A is shown in Figure 34. Analysis of the bond distances indicates that this complex is formed via an induced dipole interaction with the polarisable π-orbitals of the acetylene(ethyne) molecule. This type of study thus provides some insight into the mechanisms of interaction between adsorbate molecules and the zeolite intracrystalline surface.

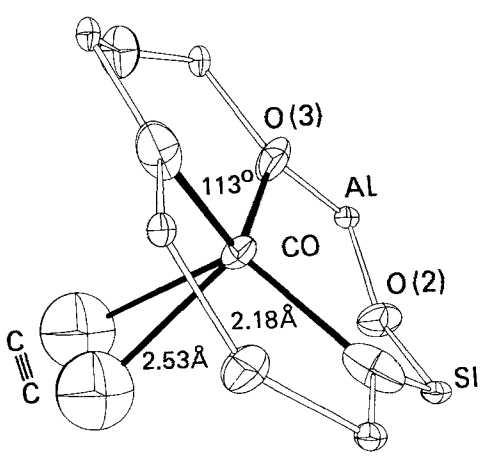

Fig. 34. Complex formation between Co^{2+} cations and acetylene in zeolite A (Adapted from [47]).

The use of the Thiele modulus concept to describe the kinetics of shape-selective catalysis [14,15,26] has already been discussed in some detail. It is to be expected that further development of this approach will continue. In fact, as more data become available on molecular intracrystalline diffusion rates in zeolites it is conceivable that the prediction of shape-selective behaviour in quantitative terms will become feasible.

A recent study which described techniques for modeling the chemistry of zeolites by means of computer graphics [52] provides a nice demonstration of a theoretical approach to shape-selective catalysis. For example, the shape-selective behaviour of ZSM-5 towards molecules such as methanol, 2,2-dimethylpentane, *p*-xylene etc. can be elegantly illustrated

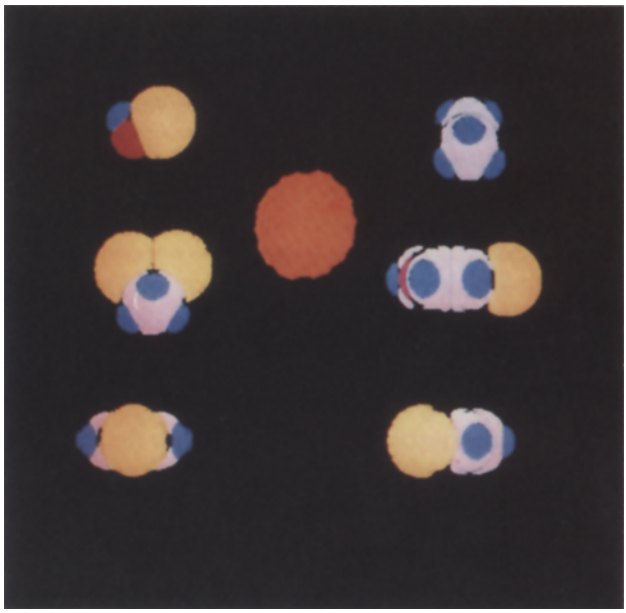

Fig. 35. Illustration of shape-selectivity of ZSM-5. The cross section of the straight channel can be compared with the size and shape of the molecules shown (approximately viewed along their molecular axis). Left, from top to bottom: methanol; 2,2-dimethylpentane; *p*-xylene. Right, from top to bottom: *n*-pentane; 4-methylquinoline; *m*-xylene (Reproduced from [52]).

using the computer graphics technique (see Figure 35). It is to be expected that these techniques will be further refined in the future, whereby, for example, various alternative transition-state complexes could be simulated within the intracrystalline space, thus providing a better understanding and improved predictive power for this type of shape selective catalysis.

The analogy between zeolite catalysis and enzyme catalytic chemistry has been discussed earlier in relation to the high level of intrinsic site activity of acidic zeolites [6]. A further analogy with biological systems can be made apparent in terms of substrate and receptor sites in enzymes. The intracrystalline space of zeolites often provide a remarkably well defined stereochemical (receptor) site for adsorbed (substrate) reactant molecules. This field of shape-selective or molecular-inclusion zeolite catalysis offers exciting possibilities, whereby catalyst systems may be designed in the future, offering a degree of chemical-reaction selectivity approaching that of enzyme systems.

Acknowledgements

The author would like to express his sincere gratitude to the following colleagues who have read the manuscript and offered valuable suggestions: Dr W. H. J. Stork and Dr R. L. Wife.

References

1. D. W. Breck: *Zeolite Molecular Sieves*, Wiley, New York (1974).
2. R. M. Barrer: *Zeolites and Clay Minerals*, Academic Press (1978).

3. J. E. D. Davies, W. Kemula, H. M. Powell, and N. O. Smith: *J. Incl. Phenom.* **1**, 3 (1983/4).
4. J. M. Thomas: *Proceedings 8th Intern. Congress on Catalysis*, Vol. I, P31, Verlag Chemie, Weinheim (1984).
5. G. R. Millward, S. Ramdas, J. M. Thomas, and M. T. Barlow: *J. Chem. Soc., Faraday Trans.* 2, **79**, 1075 (1983).
6. W. O. Haag, R. M. Lago, and P. B. Weisz: *Nature* **309**, 589 (1984).
7. J. Klinowski: *Prog. NMR Spectrosc.* **16**, 237 (1984).
8. R. M. Barrer: *J. Incl. Phenom.* **1**, 105 (1983/4).
9. P. B. Weisz: *Chemtech*, August, 498 (1973).
10. A. I. Riekert: *Am. Inst. Chem. Eng.* **17**, 446 (1971).
11. R. M. Moore and J. R. Katzer: *Am. Inst. Chem. Eng.* **18**, 816 (1972).
12. R. L. Gorring: *J. Catal.* **31**, 13 (1973).
13. Study by Gorring reported in: P. B. Weisz: *Pure Appl. Chem.* **52**, 2091 (1980).
14. M. F. Post, J. van Amstel, and H. W. Kouwenhoven: *Proceedings 6th Int. Zeolite Conference*, Reno (July 1983), P. 517.
15. W. O. Haag, R. M. Lago, and P. B. Weisz: *Faraday. Discuss. Chem. Soc.* **72**, 317 (1981).
16. P. B. Weisz and V. J. Frilette: *J. Phys. Chem.* **64**, 382 (1960).
17. P. B. Weisz, V. J. Frilette, R. W. Maatman, and E. B. Mower: *J. Catal.* **1**, 307 (1962).
18. R. M. Dessau: *J. Catal.* **77**, 304 (1982).
19. S. M. Csicsery: *J. Org. Chem.* **34**, 3338 (1969).
20. S. M. Csicsery: *J. Catal.* **19**, 394 (1970).
21. S. M. Csicsery: *J. Catal.* **23**, 124 (1971).
22. W. O. Haag, D. H. Olson, and P. B. Weisz: *Proceedings of the 29th IUPAC Congress*, 1984, 327, Pergamon Press.
23. L. D. Rollman and D. E. Walsh: *J. Catal.* **56**, 139 (1979).
24. L. D. Rollman: *J. Catal.* **47**, 113 (1977).
25. N. Y. Chen, W. W. Kaeding, and F. G. Dwyer: *J. Am. Chem. Soc.* **101**, 6783 (1979).
26. P. B. Weisz: *Pure Appl. Chem.* **52**, 2091 (1980).
27. K. Donaldson and C. R. Prout: *Proceedings Div. of Petrol. Chem., Am. Chem. Soc.* (August 1972), Paper G63.
28. J. D. Hargrove, G. J. Elkes, and A. H. Richardson: *Oil Gas J.* 104 (1979).
29. K. W. Smith, W. C. Starr, and N. Y. Chen: *Oil Gas J.* 75 (1980).
30. N. Y. Chen, R. L. Gorring, H. R. Ireland, and T. R. Stein: *Oil Gas J.* 165 (1977).
31. G. P. Hammer, and R. B. Mason: *U.S. Patent* 3575846 (1971).
32. S. P. Bund and J. Maziuk: *J. Hydrocarbon Process.* **51**, 97 (1972).
33. J. P. Grannetti, and A. J. Perrotta: *Ind. Eng. Chem., Progress Des. Div.* **14**, 86 (1975).
34. W. E. Garwood and N. Y. Chen: *Proceedings of Div. of Petrol. Chem., Am. Chem. Soc.* (March 1980), Paper P84.
35. S. L. Meisel, J. P. McCullough, C. H. Lechthaler, and P. B. Weisz: *Chemtech.* 86 (1976).
36. B. J. Miller and J. Drummond: *Petroleum Review* 32 (1981).
37. C. R. Morgan, J. P. Warner, and S. Yurchak: *Ind. Eng. Chem., Prod. Res. Dev.* **20**, 185 (1981).
38. P. Dejaifve, J. C. Vedrive, V. Bolis, J. H. C. van Hooff, and E. G. Derouane: *Proceedings Div. of Petrol. Chem., Am. Chem. Soc.* (April 1979), Paper P 286.
39. C. D. Chang and A. J. Silvestri: *J. Catal.* **47**, 249 (1977).
40. C. D. Chang, W. H. Lang, and A. J. Silvestri: *J. Catal.* **56**, 268 (1979).
41. P. B. Weisz, W. O. Haag, and P. G. Rodewald: *Science* **206**, 57 (1979).
42. J. A. Brennan, W. E. Garwood, S. Yuschak, and W. Lee: *Proceedings. Int. Seminar on Alternate Fuels*, Liège, Belgium, ed. A. Germain (1981).
43. T. Inui, T. Ishihara, N. Morinaga, G. Takeuchi, H. Matsuda, and Y. Takagami: *Ind. Eng. Chem., Prod. Res. Dev.* **22**, 26 (1983).
44. W. E. Garwood: *A.C.S. Symp. Ser. (Intracrystalline Chemistry)* **218**, 383 (1983).
45. W. O. Haag, P. G. Rodewald, and P. B. Weisz: *Preprints Div. Petr. Chem., Am. Chem. Soc.* Las Vegas Meeting (August 1980).
46. S. M. Csicsery: *Zeolites* **4**, 202 (1984).
47. I. E. Maxwell: *Adv. Catal.* **31**, 1 (1982).
48. I. E. Maxwell, R. S. Downing, and S. A. van Langen: *J. Catal.* **61**, 485 (1980).
49. I. E. Maxwell, J. J. de Boer, and R. S. Downing: *J. Catal.* **61**, 493 (1980).
50. R. M. Dessau: *J. Catal.* **89**, 520 (1984).
51. K. Seff: *Acc. Chem. Res.* **9**, 121 (1976).
52. S. Ramdas, J. M. Thomas, P. W. Betteridge, A. K. Cheetham, and E. K. Davies: *Angw. Chem. Int. Ed. Engl.* **23**, 671 (1984).